



**HAL**  
open science

# Ossements chauffés expérimentalement à basses températures : étude de la taille des particules minérales par imagerie quantitative de diffusion des rayons X aux petits angles.

Aurélien Gourrier, Oliver Bunk, K. Müller, I. Reiche

## ► To cite this version:

Aurélien Gourrier, Oliver Bunk, K. Müller, I. Reiche. Ossements chauffés expérimentalement à basses températures : étude de la taille des particules minérales par imagerie quantitative de diffusion des rayons X aux petits angles.. Archeosciences, revue d'Archéométrie, 2011, 35, pp.191-199. 10.4000/archeosciences.3137 . hal-01391451

**HAL Id: hal-01391451**

**<https://hal.science/hal-01391451>**

Submitted on 3 Nov 2016

**HAL** is a multi-disciplinary open access archive for the deposit and dissemination of scientific research documents, whether they are published or not. The documents may come from teaching and research institutions in France or abroad, or from public or private research centers.

L'archive ouverte pluridisciplinaire **HAL**, est destinée au dépôt et à la diffusion de documents scientifiques de niveau recherche, publiés ou non, émanant des établissements d'enseignement et de recherche français ou étrangers, des laboratoires publics ou privés.



Distributed under a Creative Commons Attribution - NonCommercial - ShareAlike 4.0 International License

# Artificially heated bone at low temperatures: a quantitative scanning-small-angle X-ray scattering imaging study of the mineral particle size.

Ossements chauffés expérimentalement à basses températures : étude de la taille des particules minérales par imagerie quantitative de diffusion des rayons X aux petits angles.

A. Gourrier<sup>1,2\*</sup>, O. Bunk<sup>3</sup>, K. Müller<sup>4</sup> and I. Reiche<sup>4\*\*</sup>

<sup>1</sup> Laboratoire de Physique des Solides, UMR 8502 CNRS Université Paris-Sud, 91405 Orsay, France – <sup>2</sup> European Synchrotron Radiation Facility, 38043 Grenoble, France – <sup>3</sup> Swiss Light Source, Paul Scherrer Institut, 5232 Villigen PSI, Switzerland – <sup>4</sup> Laboratoire du Centre de Recherche et de Restauration des Musées de France, UMR 171 CNRS, Palais du Louvre, 75001 Paris, France – \*To whom correspondence should be addressed – \*\* Present address: Biomaterials department, Max Planck Institute of Colloids and Interfaces, 14476 Potsdam, Germany.

**Abstract:** The ultrastructure of bovine femoral bone artificially heated at low temperatures (< 300°C) is investigated by means of synchrotron quantitative scanning-SAXS imaging. Significant changes in the distribution of particle size are observed upon heating. On average, an exponential particle growth is measured with increasing temperature independently of the tissue histology. Additionally, the heating process induces a broader dispersion in the particle size which, in turn, seems to be dependent on the bone microstructure. Those parameters could therefore be used as markers in the characterization of archaeological bone presenting traces of heating.

**Résumé:** L'ultrastructure d'échantillons d'os fémoral bovin chauffés artificiellement à basses températures (< 300°C) est analysée au moyen d'une technique de micro-imagerie par contraste de diffusion centrale des rayons X synchrotron. Des écarts significatifs dans la distribution de la taille des particules sont observés lors du chauffage. Les mesures indiquent une croissance moyenne exponentielle en fonction de la température, indépendamment des spécificités histologiques du tissu. Par ailleurs, le processus de chauffe induit une dispersion statistique importante dans la taille des particules, qui semble, en revanche, être liée aux hétérogénéités microstructurales. Ces paramètres pourraient donc servir de marqueurs dans la caractérisation d'ossements archéologiques présentant des signes de chauffage.

**Keywords:** Bone; Artificial Heating; Ultrastructure; Mineral Phase; Nanoparticle Size; Particle Growth; Synchrotron Radiation; X-ray scattering; SAXS; scanning-SAXS; quantitative SAXS imaging; qsSAXSI.

**Mots clés:** Os; Ossements; Chauffage contrôlé; Ultrastructure; Phase minérale; Taille des nanoparticules; Croissance de particules; Rayonnement synchrotron; Diffusion des rayons X; Diffusion centrale; Diffusion aux petits angles; Micro-diffusion; Imagerie quantitative par contraste de diffusion.

## Introduction.

Bone remains constitute an important part of archaeological records. Traces of heating are often observed on bone fragments and artefacts in the form of color changes and increased mechanical fragility (Stiner *et al.*, 1995; Shahack-Gross *et al.*, 1998; Weiner *et al.*, 1998; Reiche *et al.*, 2000; Chadeaux *et al.*, 2009). In many cases, however, these effects are difficult to distinguish from other diagenetic phenomena which could induce similar changes (Bennett, 1999; Reiche, 2009). In some cases, they are identified as burned on the basis of the context in which they are found on the field (e.g. urns), despite of the absence of any color changes. This often leaves unanswered a number of questions relating to the identification, conservation and understanding of the accidental or intentional origins of the heating process (Koon *et al.*, 2003, 2010). Due to the importance of this topic in the fields of archaeology, paleo-anthropology and forensic science, an important literature is available on the effect of heating on the architecture and material properties of bone-like materials, including ivory (dentin) and antler. The most important factors to consider in such investigations are the high degree of structural hierarchy and composite nature of bone. This implies, in particular, that all structural levels can be affected by heating and that the modifications in the collagen and carbonated hydroxyapatite structures may occur asynchronously. Thus, the search for specific structural patterns of heating in bone fragments should be conducted at several length scales (Reiche *et al.*, 2007; Chadeaux & Reiche, 2009).

Most studies concerned with the effect of heating have been undertaken in a large temperature range, typically in the order of  $T \sim 50 - 1000$  °C, to account for the diversity of accidental or intentional uses of fire (e.g. Shipman *et al.*, 1984; Holden *et al.*, 1995; Person *et al.*, 1996; Rogers & Daniels, 2002; Piga *et al.*, 2002; Hiller & Wess, 2006; Munro *et al.*, 2007; Lebon *et al.*, 2008, 2010). Interestingly, Kalsbeek & Richter (2006) reported that the most drastic changes in mechanical properties assessed by indentation, occur in the lowest part of that range, at  $T \sim 50 - 300$  °C. This temperature range potentially covers a wide range of socio-cultural behaviors such as cooking habits or tool manufacturing (Roberts *et al.*, 2002). At such temperatures, the color changes can be very weak, depending on the duration of heating, which makes it impractical to distinguish from non-heated fragments in the field. Furthermore, those authors show that the greatest weight loss ( $> 30$  %) and macroscopic shrinkage of the bone samples are also measured within this temperature interval. Consequently, important structural modifications are expected to occur in this range. Indeed, several studies at the microscopic scale reveal the formation of cracks which are generally correlated to other histo-morphological changes such as an increase in porosity, i.e. Haversian canals and osteocyte lacuna. This is a typical signature for a concentration of mechanical stresses within the bulk material which leads to an increased fragility of the object. Recently, Chadeaux & Reiche (2009) also provided evidence of a progressive denaturation of the collagen macromolecules using Fourier transformed infra-red (FTIR) spectroscopy in the same temperature range, which seems to be correlated with a disorganization of the mineral phase as observed by transmission electron microscopy (TEM). Similar observations have also been made in dentin (Reiche *et al.*, 2002). In the light of those elements, it is worthwhile noting that the overall picture obtained from numerous X-ray diffraction studies is that of an essentially unchanged mineral crystallinity below  $\sim 300$  °C .

In order to understand and quantify more precisely the mechanisms of such structural modifications, an investigation of the effect of a low heating treatment ( $T \sim 30 - 250$  °C) on the ultrastructure of bone was undertaken. This report presents preliminary results obtained with quantitative scanning small-angle X-ray scattering imaging (qsSAXSI) using synchrotron radiation. Small-angle X-ray scattering (SAXS) is now a well established technique for the characterization of nanoscale heterogeneities in materials (Guinier & Fournet, 1955; Glatter O. and Kratky O., 1982). With the increasing availability of synchrotron sources, this technique has become widely used for the characterization of the mineral nanoparticles in bone in the medical (e.g. Fratzl *et al.*, 1996a, 2004) and archaeological context (Wess *et al.*, 2001; Hiller *et al.*, 2003, 2004; Hiller & Wess, 2006). In this paper, we emphasize the advantages of position-resolved measurements using synchrotron sources over more standard laboratory equipment. Here the “quantitative” aspect of this imaging technique derives from the systematic analysis of the 2D SAXS patterns obtained as a function of scan position, as opposed to more widely known SAXS imaging techniques which use scattering effects to enhance the contrast in a more qualitative way, be it in scanning (e.g. Bunk *et al.*, 2009) or in full-field (e.g. Levine *et al.*, 2004) mode.

## Methods.

**Sample preparation:** The samples were prepared from modern bovine tibia obtained from a local butcher. The periosteum and marrow were mechanically removed and a transverse cross-section of  $\sim 15$  mm in thickness was sawn in the diaphysis, defatted for 24 h in acetone and dried in air at room temperature for 48 h. The anterior and posterior cortical blocks were then selected and 7 sections of 200  $\mu\text{m}$  in thickness and  $\sim 10 \times 10$  mm<sup>2</sup> in width and length were cut from each block in the transverse direction using a high precision low-speed diamond saw (Accutome 5, Struers Tech A/S, Copenhagen, Denmark). These were reduced in thickness to  $60 \pm 4$   $\mu\text{m}$  by polishing with high grade SiC paper (2400) using a custom device designed to obtain well controlled parallel surfaces within  $\pm 1$   $\mu\text{m}$ . From each of the two series (anterior and posterior), one section was kept as a reference (so-called unheated) while the six remaining were heated at 100°C, 150°C, 170°C, 190°C, 210°C, 250°C in a domestic oven during 1 h to obtain a homogeneous temperature gradient within the sample. Although far from field-conditions, this procedure allows avoiding artifacts caused by temperature gradients in bulk samples or other effects linked with the presence of lipids.

**Scanning-SAXS experiments:** The scanning-SAXS experiments were performed at the cSAXS beamline of the Swiss Light Source, Paul Scherrer Institut, Villigen, Switzerland (Bunk *et al.*, 2009). The X-ray beam was monochromated to a wavelength of  $\lambda = 0.667$  Å ( $E = 18.58$  keV) using a Si(111) double-crystal monochromator. A horizontal and vertical focus at sample position of  $\sim 25 \times 6$   $\mu\text{m}$  (FWHM) was achieved using the second (bending) mirror of the monochromator and an additional bending mirror, respectively. The photon flux at focal position was in the order of  $5 \times 10^{10}$  ph.s<sup>-1</sup>. The samples were mounted between two thin Kapton<sup>®</sup> foils (25  $\mu\text{m}$  thick) glued on an aluminium support frame fixed on a high-precision translation stage and visualized using an off-axis microscope to select the areas of interest. Each sample was scanned over the full cortical thickness ( $\sim 11.5$  mm) and 1.5–2 mm across with a step size of  $50 \times 20$   $\mu\text{m}^2$  in horizontal and vertical directions. The SAXS patterns were collected with an exposure time of 100 ms and read-out time of 20 ms using a Pilatus 2M detector at full resolution, *i.e.*  $1475 \times 1679$  pixels of  $172 \times 172$   $\mu\text{m}^2$ . The parasitic scattering was reduced using a 2.1 m evacuated flight tube between the sample and the detector, and the sample-to-detector distance, detector tilt and the beam centre were calibrated using a silver behenate standard (Blanton *et al.*, 1995). This configuration provided a measurable  $q$ -range of 0.01–4.1 nm<sup>-1</sup> where  $q$  is the norm of the scattering vector  $q = 4\pi\sin\theta/\lambda$  and  $\theta$  is the scattering angle.

**Data analysis:** The two dimensional SAXS patterns were spherically integrated along the azimuthal and radial directions using the FIT2D software package (Hammersley, 1997). The one dimensional profiles were subsequently analyzed using a dedicated SAXS analysis library written in Python language by one of the authors (A. Gourrier), which is optimized for the analysis of large data sets. Several structural parameters relating to the mineral nanoparticle thickness, lateral organization and orientation can thus be determined following procedures established by Fratzl *et al.* for bone studies (see, e.g. Fratzl *et al.*, 1996). The average chord length (so-called  $T$  parameter) can be considered as a standard parameter in the SAXS analysis of bone in the archaeological context. This parameter can be expressed as the ratio of volume fraction of mineral  $\Phi$  to the total mineral/organic interface  $\sigma$ :  $T = 4\Phi(1 - \Phi)/\sigma$ . Under the assumption of a 50 % volume fraction of mineral phase, Fratzl *et al.* (1991, 1992, 1996a) have shown that  $T$  gives a direct measure of the nanoparticle thickness. In the present work,  $T$  was calculated using a recent method, which allows overcoming the limitations in the detection of the SAXS signal at low scattering angles. A detailed description of this model is outside the scope of the present paper but can be found in Fratzl *et al.* (2005) and Gourrier *et al.* (2010). In brief, this method involves fitting the profile  $Iq^2$  vs  $q$  ( $I$  is the measured scattered intensity) with an analytical expression which is a function of  $T$ . This method is in direct line with previous work by Wess *et al.* (2001), in particular, who assessed the deviation from an idealized Lorentzian profile in order to assess the spatial correlation between mineral particles. In this way quantitative images of  $T$  can be reconstructed as a function of scan position (Fratzl *et al.*, 1997; Riekel *et al.*, 2000, Paris *et al.*, 2008; Gourrier *et al.*, 2007, 2010).

## Results.

An optical micrograph of the reference sample is shown in Fig.1.a. Typical histological features can be observed in Fig.1.b the form of osteons (O), bone packets (P) as well as Haversian canals (H) and osteocyte lacunae which appear as small dark spots on the image. The scanned area is indicated by a solid rectangle in Fig.1.a is  $\sim 1.5$  (h)  $\times$  11.5 (v)  $\text{mm}^2$  and covers the full cross-section from the endostum (bottom) to the periostum (top). The red filled rectangle in Fig.1.b represents the scan step of the measurement, i.e. 50 (h)  $\times$  20 (v)  $\mu\text{m}^2$  enlarged by a factor of 2 for clarity. Since the X-ray beam is smaller in dimensions, those values ultimately define the spatial resolution limits. A composite image of the SAXS patterns obtained in a small part of the scan indicated by the white rectangle in Fig.1.a is shown in Fig.1.c. The SAXS signal has an elliptic shape which is typical of bone and reflects the shape and arrangement of the mineral platelets: more elongated ellipses indicate that the nanoparticles are aligned along a preferred direction, while circular patterns point to a random orientation in the volume of the beam (Fratzl *et al.*, 1996a). In order to compare the data with those obtained with more widely used laboratory equipment, the same data were averaged over areas of 100 (h)  $\times$  100 (v)  $\mu\text{m}^2$  and over the full region (1 (h)  $\times$  0.5 (v)  $\text{mm}^2$ ) and are shown in Fig1.d,e respectively. The first corresponds to the typical spatial resolution of an instrument with microfocus capability while the second is closer to standard X-ray source dimensions. It can be observed that the SAXS signal becomes more circular upon enlarging the illuminated area. This implies that, although the mineral platelets are locally well aligned, on average, there isn't any privileged direction in the orientation of the nanoparticles.

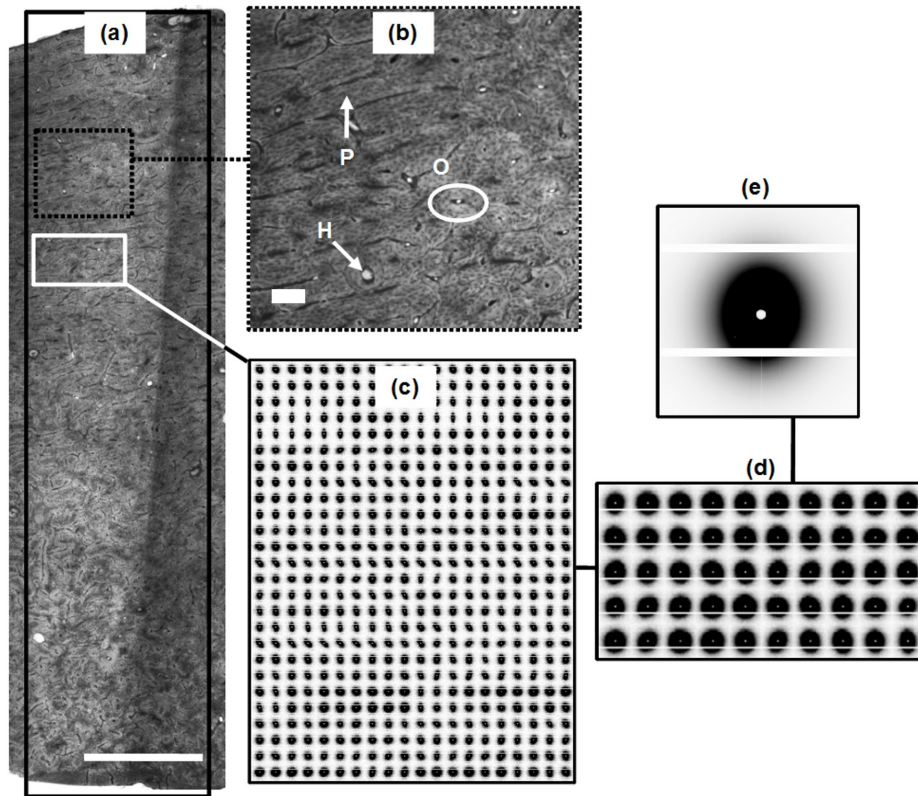


**Fig.1:** (a) optical micrograph of the reference sample in the posterior region. The scanned area is indicated by the solid black rectangle and the scale bar at the bottom represents 1 mm. At higher magnification, typical histological features are observed (b) such as osteons (O) and Haversian canals (H) as well as bone packets (P). The red filled rectangle in (b) represents the scan steps (50 (h)  $\times$  20 (v)  $\mu\text{m}^2$ ) enlarged by a factor of 2 for clarity. (c) composite image of the 2D SAXS patterns in a small part of the scan indicated by a white rectangle in (a) (950 (h)  $\times$  500 (v)  $\mu\text{m}^2$ ). (d) similar image of 2D SAXS patterns averaged over 100 (h)  $\times$  100 (v)  $\mu\text{m}^2$  areas within the same region. (e) average SAXS pattern for the whole scanned region.

In order to assess the global changes within the samples as a function of heating temperature, the average SAXS patterns were calculated for the whole scanned region and azimuthally integrated. The corresponding Kratky plots ( $Iq^2$  vs.  $q$ ) are shown in Fig.2.

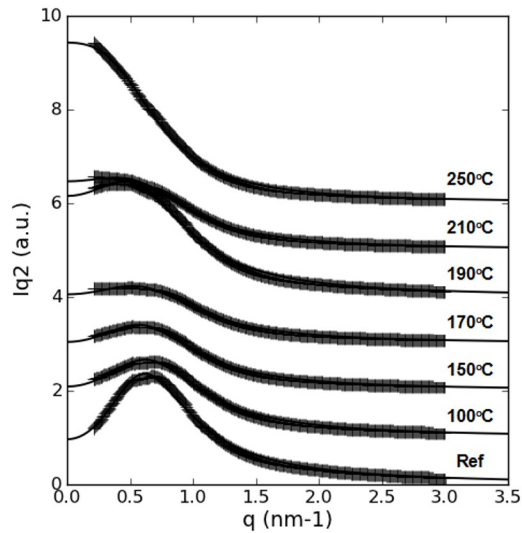


**Fig.2:** Kratky plots ( $Iq^2$  vs.  $q$ ) of the azimuthally integrated intensity of the averaged 2D SAXS patterns as a function of temperature for the posterior sections.

Significant differences can be observed in the form of a progressive shift of the maximum of the Kratky curves towards lower values of  $q$  up to a total disappearance of the maximum at 250°C. Similar observations were made in a previous study on human fluorotic bone pointing towards a greater disorder in the mineral nanoparticle thickness and inter-particle distance (Fratz *et al.* 1996b; Gourrier *et al.*, 2010). The values of  $T$  calculated from the fit of those curves are shown as a function of temperature in Fig.3. A clear trend can be observed in form of an exponential increase of  $T$ . Providing that the collagen volume fraction remains unchanged, the physical interpretation of this trend is a general increase in particle thickness. The hypothesis of a constant volume fraction of organic molecules is well supported by FTIR results obtained in similar conditions by Chadeaux & Reiche (2009) who showed that, although there is a progressive denaturation of the collagen molecules, the total area of the Amide peaks in the FTIR spectra remains essentially constant up to 230°C.

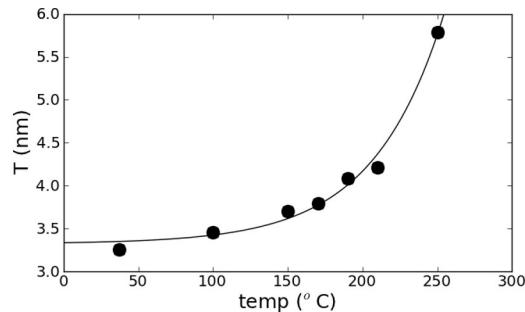


**Fig.3:** Evolution of  $T$  calculated from the Kratky curves shown in Fig.2 as a function of temperature.

In order to understand the modifications at the tissue level, the values of  $T$  were calculated for each 2D SAXS pattern of the scan. The corresponding images for the posterior sections are shown in Fig.4 for each temperature on the same color scale. A clear increase in  $T$  is observed in the form of an overall increase in brightness which is particularly striking between 210°C and 250°C. A closer examination allows to distinguish the histological features observed in Fig.1.a,b, i.e. osteons and interstitial bone or bone packets. The relative density of osteons appears to fluctuate between the different sections and reflects the sample heterogeneity. Thus, a direct comparison using image registration methods is not possible.

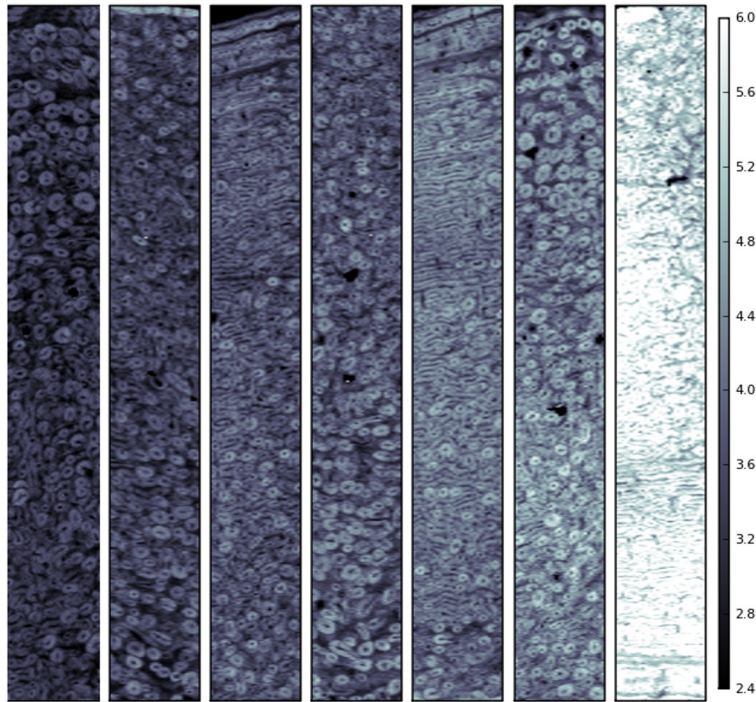


**Fig.4:** Images of  $T$  for the posterior sections as a function of temperature. All images are displayed on the same color scale for comparison.

To compare the information contained in the images, the histogram of the images was calculated using bins of  $\Delta T = 0.1$  nm. The result is shown in Fig.5, where the histograms represent the  $T$  distribution in percentage of the total bone area, i.e. disregarding the parts of the images corresponding to Haversian canals or other form of voids which appear in black in Fig.4. For clarity, the histograms for the sections heated at 150°C and 190°C are not shown. The  $T$  distributions appear Gaussian in shape. The position of the maximum of the curve can therefore be viewed as the average  $T$  value, while the breadth of the curve, which is generally characterized by its full-width at half maximum (FWHM), provides an indication on the dispersion about the mean value. A clear trend can be observed in the form of a shift towards higher values of  $T$  with increasing temperature which is correlated with a decrease of the maximum and a broadening of the histograms.

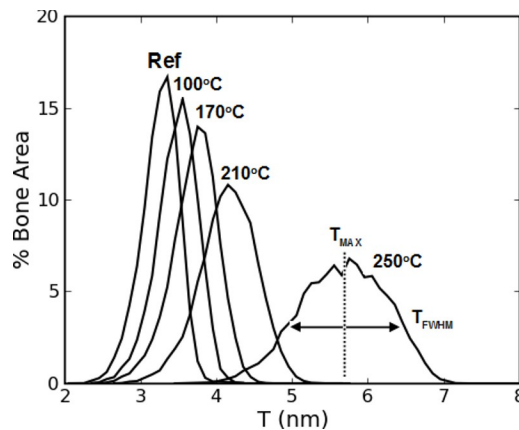


**Fig.5:** Histograms of the images shown in Fig.4 (for clarity, the histograms at 150°C and 190°C are not shown). The  $T$  distribution can be characterized, in first approximation, by the position of the maximum ( $T_{MAX}$ ) and by its full width at half-maximum ( $T_{FWHM}$ ).

Interestingly, the shift in peak position between 210°C and 250°C is approximately twice that measured between 37°C (reference) and 210°C which clearly suggests a non-linear trend. To quantify this evolution, the position of the maximum ( $T_{MAX}$ ) and the FWHM ( $T_{FWHM}$ ) of the curves were measured (Fig.5). These parameters can be related to the mean and the variance of the  $T$  distribution. We recall here that, for a Gaussian function the FWHM =  $2\sqrt{2\ln 2}\cdot\sigma$  where  $\sigma$  is the standard deviation and  $\sigma^2$  the variance of the distribution. It is well known in statistics that those values correspond to the moments of order 0 and 2 which are sufficient to fully characterize Gaussian distributions. The result of these calculations for the anterior and posterior sections is shown in Fig.6. Both  $T_{MAX}$  (Fig.6.a) and  $T_{FWHM}$  (Fig.6.b) rise exponentially with increasing temperatures. However, a significant distinction can be made between the results obtained for the anterior (black circles) and posterior (white triangles) sections in  $T_{FWHM}$  which is not observed in  $T_{MAX}$ . This suggests that the increase in average particle thickness is similar for the anterior and posterior samples but that there is a greater dispersion (variance) in particle size distribution.

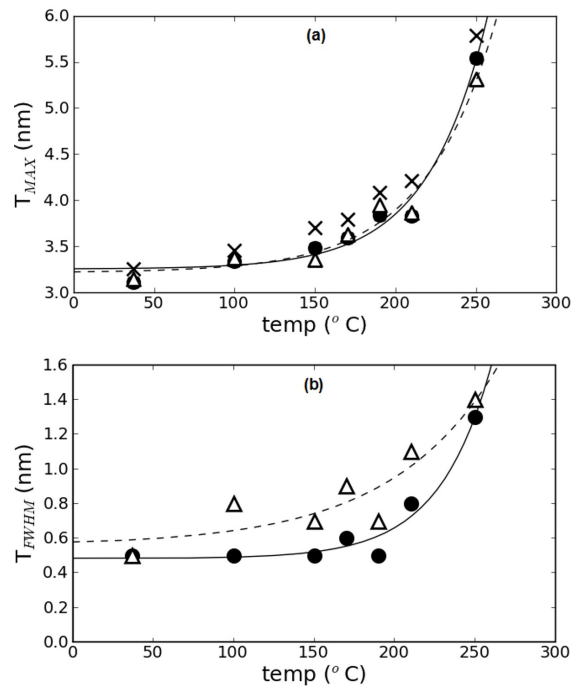


**Fig.6:** Evolution of  $T_{MAX}$  (a) and  $T_{FWHM}$  (b) as a function of temperature. The results for the anterior and posterior sections are shown respectively in solid black circles and white triangles. The values of  $T$  shown in Fig.3 are also indicated in the form of crosses.

## Discussion.

From the previous considerations, several important conclusions can be drawn. First, there is a clear increase in average particle thickness upon heating even at relatively low temperature below 300 °C, as observed by the exponential raise of  $T_{MAX}$  in Fig.6.a. This is in agreement with other studies on the evolution of the mineral phase upon heating observed at temperatures higher than 300 °C (e.g. Hiller & Wess, 2004, 2006). Secondly, there is also a significant increase in  $T_{FWHM}$  (Fig.6.b) and, hence, in the variance of the  $T$  distribution. This means that the particle growth process is heterogeneous throughout the tissue. This also confirms first observations by TEM (Chadefaux *et al.*, 2009). Third, although the global trends are exponential in all cases, there is a significant difference in the evolution of  $T_{FWHM}$  between the anterior and posterior samples. This must be put in perspective with the histological differences between the two, which are known to be related to different biomechanical behaviors, the posterior section generally being loaded in compression mode while the anterior section is mostly submitted to tensile stresses (Currey, 2002).

From the archaeological perspective, this has important practical consequences in the characterization of heated bone remains. Probably most important, the average mineral particle size appears to be a valuable marker for the determination of the heating temperature. For this purpose, it is worthwhile noting that standard laboratory SAXS equipment is sufficient. This is illustrated in Fig.5.a. where the values of  $T$  obtained from the averaged SAXS profile for the whole scan (crosses) are very close to  $T_{MAX}$  for the anterior and posterior sections. However, our results also demonstrate that very valuable information can be obtained using synchrotron qSAXSI with higher spatial resolution (i.e. smaller beam size) since the images of  $T$  can be related to the histological features observed using other modalities, e.g. light microscopy. Furthermore, the histogram of the image provides the full  $T$  distribution which can be analyzed following classical methods used in other imaging techniques. In the present study, we propose an additional parameter,  $T_{FWHM}$  which characterizes the breadth of the  $T$  distribution and is found to be dependent on the sample histology. It can therefore be postulated that samples with different microstructures will yield different values of  $T_{FWHM}$ . This requires some caution since the experiment was essentially limited to a single heating time although it is generally admitted that 1 h heating is enough to reach equilibrium. It could be hypothesized, for instance, that the offset in  $T_{MAX}$  and  $T_{FWHM}$  is dependent on the duration of heating. It is also worthwhile mentioning that there exists a number of laboratory equipment providing positional resolution with beam sizes in the order of 100  $\mu\text{m}$  in diameter. This represents an improvement with respect to more standard equipment and could provide a reasonable description of the  $T$  distribution but is still insufficient to resolve the histological features (secondary osteons are generally in the range of 50 – 100  $\mu\text{m}$  in diameter). Therefore, a detailed assessment of the effect of heating requires beam sizes of  $\sim 10 - 20 \mu\text{m}$  in diameter at maximum. For archeological artefacts, where the effects of diagenesis are often heterogeneous, this requirement appears even more stringent. In seminal work by Hiller & Wess (2004, 2006) on a varied set of archaeological artefacts, significant correlations were found between the SAXS measurement of  $T$  and other diagenetic markers deduced from Fourier-transformed infrared spectroscopy, such as splitting factor and carbonate:phosphate ratio. However, an important dispersion in the data was observed, which led the authors to postulate the co-existence of several populations of particles with different sizes. We believe that this is a very strong hypothesis which emphasizes the necessity of taking into account the specific histological features of the different samples. This, therefore, highlights the potential of our analytical strategy for further studies of bone heated in conditions closer to those encountered in the archaeological context.

Finally, a number of X-ray diffraction studies show that substantial differences in diffraction spectra can only be observed above 300 – 400  $^{\circ}\text{C}$  in the form of a progressive narrowing of the X-ray peaks indicating an increase in crystallinity and particle size (Piga et al., 2008; Rogers et al., 2002, 2010; Kalsbeek & Richter, 2006). Below these temperatures, the profiles only reveal minor modifications, which are difficult to interpret. The picture for the SAXS analysis is exactly the inverse: below these temperatures, the result obtained in the present study clearly provides a quantitative description of the mineral particle thickness evolution, while the interpretation of the SAXS spectra above these temperatures is complicated due to the degradation of collagen. Therefore, SAXS should be preferred to XRD for the structural characterization of low temperature heating effects, and *vice versa*.

## Conclusion.

This study demonstrates that the thickness of the mineral nanoparticles follows an exponential increase upon heating at temperatures below 300  $^{\circ}\text{C}$  and can therefore be considered as a potential valuable marker to understand the processes of heating to which bone remains have been submitted. The use of position resolved measurements for quantitative scanning-SAXS imaging provides additional information related to the histology of the sample, which could allow further discriminating between species and bone types. Finally, we suggest that SAXS measurements are preferable to X-ray diffraction for the characterization of bone submitted to low heating temperatures, i.e. below  $\sim 300 \text{ }^{\circ}\text{C}$ . Further studies should clarify the influence of the duration of heating on the extent of growth in particle size through isothermal measurements. Ultimately, changes induced by diagenetic processes also need to be investigated in relation with our findings.

## Acknowledgements.

The authors would like to acknowledge the ANR for financial support (ArBoCo project; contract number: ANR-07-JCJC-0149) and Céline Chadeaux for preliminary work and help in the sample preparation.

## References.

- Bennett, J.L., 1999. *Thermal Alteration of Buried Bone*. Journal of Archaeological Science. 26: 1-8.
- Blanton, T. N. Huang, T. C., Toraya, H., Hubbard, C. R., Robie, S. B., Louër, D., Göbel, H. E., Will, G., Gilles, R. and Raftery, T., 1995. *A possible low-angle X-ray diffraction calibration standard*. Powder Diffraction. 10: 91-95.
- Bunk, O., Bech, M., Jensen, T.H., Feidenhans, R., Binderup, T., Menzel, A. and Pfeiffer F., 2009. *Multimodal x-ray scatter imaging*. New Journal of Physics, 11 : 123016.
- Chadeaux, C., Vignaud, C., Chalmin, E., Robles-Camacho, J., Arroyo-Cabrales, J., Johnson, E. and Reiche, I., 2009. *Color origin and heat evidence of paleontological bones: Case study of blue and gray bones from San Josecito Cave, Mexico*. American Mineralogist. 94: 27–33.
- Chadeaux, C. and Reiche, I., 2009. *Archaeological bone from macro- to nanoscale. Heat-induced modifications at low temperatures*. Journal of NanoResearch, 8: 157-172.
- Currey, J. D., 2002. *Bones: Structure and Mechanics*. Princeton University Press.
- Fratzl, P., Fratzl-Zelman, N., Klaushofer, K., Vogl, G. & Koller, K., 1991. *Nucleation and growth of mineral crystals in bone studied by small-angle X-ray scattering*. Calcified Tissue International. 48: 407–413.
- Fratzl, P., Groschner, M., Vogl, G., Plenk, H. Jr, Eschberger, J., Fratzl-Zelman, N., Koller, K. & Klaushofer, K., 1992. *Mineral crystals in calcified tissues: a comparative SAXS study*. Journal of Bone and Mineral Research. 7: 329–334.
- Fratzl, P., Schreiber, S., Klaushofer, K., 1996a. *Bone Mineralization as Studied by Small-Angle X-Ray Scattering*. Connective Tissue Research. 34: 247-254.
- Fratzl, P., Schreiber, S., Roschger, P., Lafage, M.H., Rodan, G. and Klaushofer, K., 1996b. *Effects of Sodium Fluoride and Alendronate on the bone mineral in minipigs: a small-angle X-ray scattering and backscattered electron imaging study*. Journal of Bone and Mineral Research. 11: 248–253.
- Fratzl, P., Jakob, H.F., Rinnerthaler, S., Roschger, P. and Klaushofer, K., 1997. *Position-resolved Small-angle X-ray scattering of complex biological materials*. Journal of Applied Crystallography. 30: 765-769.
- Fratzl, P., Gupta, H.S., Paschalis, E.P., Roschger, P., 2004. *Structure and mechanical quality of the collagen-mineral nanocomposite in bone*. Journal of Materials Chemistry. 14: 2115-2123.
- Fratzl, P., Gupta, H. S., Paris, O., Valenta, A., Roschger, P. and Klaushofer, K., 2005. *Diffracting “stacks of cards” – some thoughts about small-angle scattering from bone*. Progress in Colloid and Polymer Science. 130: 33–39.
- Glatter, O. and Kratky, O., 1982. Editors. *Small-Angle X-ray Scattering*. New York: Academic Press.
- Gourrier, A., Wagermaier, W., Burghammer, M., Lammie, D., Gupta, H.S., Fratzl, P., Riekel, C., Wess, T.J. and Paris, O., 2007. Journal of Applied Crystallography. 40: s78–s82.
- Gourrier, A., Li, C., Siegel, S., Paris, O., Roschger, P., Klaushofer, K. and Fratzl, P., 2010. *Scanning small angle X-ray scattering analysis of the size and organization of the mineral nanoparticles in fluorotic bone using a stack of cards model*. Journal of Applied Crystallography. 43: 1385-1392.
- Guinier A. and Fournet G., 1955. *Small-angle scattering of X-rays*. J. Wiley & sons.
- Hammersley, A.P., 1997. ESRF Internal Report No. ESRF97, HA02T. European Synchrotron Radiation Facility, Grenoble, France.
- Hiller, J.C., Thompson, T.J.U., Evison, M.P., Chamberlain, A.T., Wess, T.J., 2003. *Bone mineral change during experimental heating: an X-ray scattering investigation*. Biomaterials, 24: 5091-5097.
- Hiller, J.C., Collins, M.J., Chamberlain, A.T., Wess, T.J., 2004. *Small-angle, X-ray scattering: a high-throughput technique for investigating archaeological bone preservation*. Journal of Archaeological Science. 31: 1349-1359.
- Hiller, J.C. and Wess, T.J., 2006. *The use of small-angle X-ray scattering to study archaeological and experimentally altered bone*. Journal of Archaeological Science. 33: 560-572.
- Holden, J.L., Phakey, P.P., Clemental, J.G., 1995. *Scanning electron microscope observations of heat-treated human bone*.

Forensic Science International. 74: 29-45.

Kalsbeek, N. and Richter, J., 2006. *Preservation of burned bones: an investigation of the effects of temperature and pH on hardness*. Studies in Conservation, 51 : 123-238.

Koon, H.E.C., Nicholson, R.A. and Collins, M.J., 2003. *A practical approach to the identification of low temperature heated bone using TEM*. Journal of Archaeological Science, 37: 62–69.

Koon, H.E.C., O'Connor, T.P. and Collins, M.J., 2010. *Sorting the butchered from the boiled*. Journal of Archaeological Science, 37: 62–69.

Lebon, M., Reiche, I., Fröhlich, F., Bahain, J.-J., Falguères, C., 2008. *Characterization of archaeological burnt bones: contribution of a new analytical protocol based on derivative FTIR spectroscopy and curve fitting of the  $\nu_{13}$  PO<sub>4</sub> domain*. Analytical and Bioanalytical Chemistry. 392: 1479-1488.

Lebon, M., Reiche, I., Bahain, J.-J., Chadeaux, C., Moigne, A.-M., Fröhlich, F., Sémah, F., Schwartz, H.P., Falguères, C., 2010. *New parameters for the characterization of diagenetic alterations and heat-induced changes of fossil bone mineral using Fourier transform infrared spectrometry*. Journal of Archaeological Science. 37: 2265-2276.

Levine, L.E. and Long, G.G., 2004. *X-ray imaging with ultra-small-angle X-ray scattering as a contrast mechanism*. Journal of Applied Crystallography. 37: 757-765.

Munro, L.E., Longstaffe, F.J. and White, C.D., 2007. *Burning and boiling of modern deer bone: Effects on crystallinity and oxygen isotope composition of bioapatite phosphate*. Palaeogeography, Palaeoclimatology, Palaeoecology. 249: 90-1002.

Paris, O., 2008. *From diffraction to imaging: New avenues in studying hierarchical biological tissues with x-ray microbeams*. Biointerphases. 3: FB16-FB26.

Person, A., Bocherens, H., Mariotti, A., Renard, M., 1996. *Diagenetic evolution and experimental heating of bone phosphate*. Palaeogeography, Palaeoclimatology, Palaeoecology. 126: 135-149.

Piga, G., Malgosa, A., Thompson, T.J.U., Enzo, S., 2008. *A new calibration of the XRD technique for the study of archaeological burned human remains*. Journal of Archaeological Science. 35: 2171-2178.

Pijoan, C. MA., Mansilla, J., Leboeiro, I., Lara, V.H. and Bosch, P., 2007. *Thermal alterations in archaeological bones*. Archaeometry. 49 : 713-727.

Reiche, I., Vignaud, C. and Menu, M., 2000. *Heat induced transformation of fossil mastodon ivory into turquoise "odontolite". Structural and elemental characterisation*. Solid State Sciences. 2: 625-636.

Reiche, I., Vignaud, C. and Menu, M., 2002. *The crystallinity of Ancient Bone and Dentine: New insights by Transmission Electron Microscopy*. Archaeometry. 44: 447-459.

Reiche, I., Chadeaux, C., Vignaud, C. Menu, M., 2007. *Les matériaux osseux archéologiques Des biomatériaux nanocomposites complexes*. l'actualité chimique. 312-313: 86-92.

Reiche, I., 2010. *Heating and diagenesis-induced heterogeneities in the chemical composition and structure of archaeological bones from the Neolithic site of Chalain 19 (Jura, France)*. In : The taphonomy of burned organic residues and combustion features in archaeological contexts, Théry-Parisot I., Chabal L. & Costamagno S. (eds). Proceedings of the round table, Valbonne, May 27-29 2008. P@lethnologie, 2: 129-144.

Riekel, C., 2000. *New avenues with X-ray microbeam experiments*. Reports on progress in physics. 63: 233-262.

Roberts, S.J., Smith, C.I., Millard, A., Collins, M.J., 2002. *The taphonomy of cooked bone: characterizing boiling and its physico-chemical effects*. Archaeometry. 3: 485-494.

Rogers, K.D. and Daniels, P., 2002. *An X-ray diffraction study of the effects of heat treatment on bone mineral structure*. Biomaterials, 23: 2577-2585.

Shahack-Gross, R., Bar-Yosef, O. and Weiner, S., 1997, *Black-Coloured Bones in Hayonim Cave, Israel: Differentiating between Burning and Oxide Staining*. Journal of Archaeological Science, 24: 439-446.

Shipman, P., G. Foster, and M. Schoeninger, *Burnt Bones and Teeth: an Experimental Study of Color, Morphology, Crystal Structure and Shrinkage*. Journal of Archaeological Science, 1984. 11: p. 307-325.

Stiner, M.C., Kuhn, S.L., Weiner, S., Bar-Yosef, O., 1995. *Differential Burning, Recrystallisation, and Fragmentation of Archaeological Bone*. Journal of Archaeological Science, 22: 223-237.

Thompson, T.J.U., Gauthier, M., Islam, M., 2009. *The application of a new method of Fourier Transform Infrared Spectroscopy to the analysis of burned bone*. Journal of Archaeological Science, 36: 910-914.

Weiner, S., Xu, Q., Goldberg, P., Liu, J., Bar-Yosef, O., 1998. *Evidence for the Use of Fire at Zhoukoudian, China*. Science, 281: p. 251-253.

Wess, T.J., Drakopoulos, M., Snigirev, A., Wouters, J., Paris, O., Fratzl, P., Collins, M., Hillier, J. and Nielsen, K., 2001. *The use of small angle X-ray diffraction studies for the analysis of structural features in archaeological samples.* Archaeometry. 43: 117-129.